The Journal of Adhesion, 82:447–468, 2006

ISSN: 0021-8464 print/1545-5823 online
DOI: 10.1080/00218460600713592

Taylor & Francis
Taylor & Francis Group

Effect of Interfacial Adhesion on the Mechanical Properties of Organic/Inorganic Hybrid Nanolaminates

Bongjun Yeom
Suhan Kim
Jinhan Cho
School of Chemical and Biological Engineering and
Nano Systems Institute—National Core Research Center,
Seoul National University, Seoul, Korea

Junhee Hahn
Korea Research Institute of Standards and Science, Daejeon, Korea

Kookheon Char
School of Chemical and Biological Engineering and
Nano Systems Institute—National Core Research Center,
Seoul National University, Seoul, Korea

Two different kinds of organic polyelectrolyte (PE)/inorganic silicate nanolaminates carrying dissimilar interfacial adhesion between the organic and the inorganic layers were prepared using the layer-by-layer self-assembly. To investigate the mechanical behavior of the prepared hybrid films, apparent modulus (E′), hardness (H), and crack length were measured by depth-sensing nanoindentation as well as a microVickers experiment. The fracture toughness of the hybrid films was then calculated based on the measured mechanical values. In the case of forming strong interfacial adhesion between the organic and the inorganic layers (A series), the fracture toughness and the crack resistance of hybrid multilayer films were significantly improved as a result of the redistribution of stress concentration and the dissipation of fracture energy by the plasticity of organic PE layers. On the other hand, samples with relatively low interfacial adhesion between the organic and the inorganic layers (T series) had little effect on the improvement of fracture toughness of the hybrid films.

Received 8 October 2005; in final form 13 March 2006.

One of collection of papers honoring Hugh R. Brown, who received *The Adhesion Society Award for Excellence in Adhesion Science, Sponsored by 3M*, in February 2006.

Address correspondence to Kookheon Char, School of Chemical and Biological Engineering, Seoul National University, Seoul 151-744, Korea. E-mail: khchar@plaza.snu.ac.kr

Present address of Jinhan Cho is School of Advanced Materials Engineering, Kookmin University, Jeongneung-dong, Seongbuk-gu, Seoul, 136-702, Korea.

Keywords: Fracture toughness; Interfacial adhesion; Mechanical property; Nacre; Nanoindentation; Organic/inorganic hybrid nanolaminate

INTRODUCTION

It is well known that the nacres of abalone shells, because of the sandwich structure of 200–900 nm $CaCO_3$ blocks (*i.e.*, a hard inorganic component) and 10–40-nm-thick organic protein-polysaccharide matrix (*i.e.*, a soft organic layer), have mechanical properties superior to many manmade organic/inorganic (nano)composites [1–5]. This unique structure of the nacres yields approximately a twofold increase in mechanical strength and a thousandfold increase in fracture toughness when compared with a single inorganic layer [1–7]. It has also been reported that the organic component occupying merely 5 wt% of the nacre significantly improves the fracture toughness of nacres because the organic layers with fibrous morphology are believed to hold the $CaCO_3$ platelets together electrostatically [8–11]. These reported results imply that the interfacial adhesion between the organic and inorganic layers can have a significant influence on the absorption of applied deformation energy in view of fracture toughness [5,6,8]. As a result, many researchers have tried to elucidate how the novel structure is constructed in nature and to improve mechanical properties of artificial hybrid materials through mimicking the internal structure and the adhesion properties of seashell nacres [12–21]. Obviously, this line of research could give new insights into many industrially important areas involving novel hard coatings, synthetic hard tissue for biological applications, and nanocomposites.

Decher *et al.* introduced the layer-by-layer (LbL) self-assembly (SA) technique based on the dipping process (*i.e.*, dip SA) to produce multilayer films in 1992 [22–24]. This dip SA method was later extended to the spin SA method, yielding a sharp interface between adjacent layers as well as extremely smooth surface roughness [25,26]. The LbL films formed through either electrostatic interactions or hydrogen bonding have been widely applied to devices with unique electrical, optical, or biological properties [25–42]. In particular, organic/inorganic multilayer films prepared by the LbL method have attracted much interest in realizing nanocomposite films similar to the internal structure of the nacres [43–45]. Tang *et al.* reported that organic/inorganic multilayers consisting of montmorillonite clay platelets and polyelectrolytes (PE) can be prepared by the dip SA method, and the mechanical properties of these films are similar to those of nacres in terms of tensile strength and ultimate Young's modulus

[44]. However, they did not investigate the fracture toughness of organic/inorganic hybrid nanolaminates although high fracture toughness is the most important and remarkable feature of the nacres. Also, there has been no systematic study on the effects of interfacial adhesion on the fracture toughness of organic/inorganic hybrid nanolaminates.

In this study, we systematically investigate the effect of interfacial adhesion between organic and inorganic layers on the fracture toughness. For this investigation, organic/inorganic multilayer films were prepared with (organo)silicate oligomers (precursors) as an inorganic layer in combination with PE multilayers as an organic layer. Although the inorganic precursor is deposited by dip coating, the PE organic multilayers are deposited onto a substrate by the spin SA method. This combination of dip coating and spin SA method allows us to prepare hybrid multilayer films with relatively thick inorganic layers as well as with highly ordered internal structure. In the present case, the electrostatic interaction between PE and silicate layers, as well as between adjacent PE layers, was employed in varying degree for the buildup of hybrid multilayer films. To investigate the effect of interfacial adhesion between the PE and the silicate layers on the fracture toughness more specifically, two different kinds of films were prepared as follows: T_n series with weak electrostatic interaction between PE and silicate layers, and A_n series with relatively strong electrostatic interaction compared with the T_n series. Fracture toughness of both series was estimated based on the measured values of apparent modulus (E') and hardness (H) obtained from depth-sensing nanoindentation as well as the crack length measured from a microVickers experiment [46–51]. We believe that the present work has important implications in that the plasticity of inserted organic layers could cause the relaxation of stress concentration in response to the applied deformation energy when the interfacial adhesion is fairly high.

EXPERIMENTAL

Materials

Tetraethoxysilane (TEOS), 3-aminopropyltriethoxysilane (3-APTES), poly(diallyldimethylammonium chloride) (PDAC) ($M_w = 200000$–350 000), and poly(sodium 4-styrenesulfonate) (PSS) ($M_w = 70000$) were used as received from Sigma-Aldrich Korea, Yougin City, Korea. The chemical structures of the compounds used in our work are schematically shown in Figure 1.

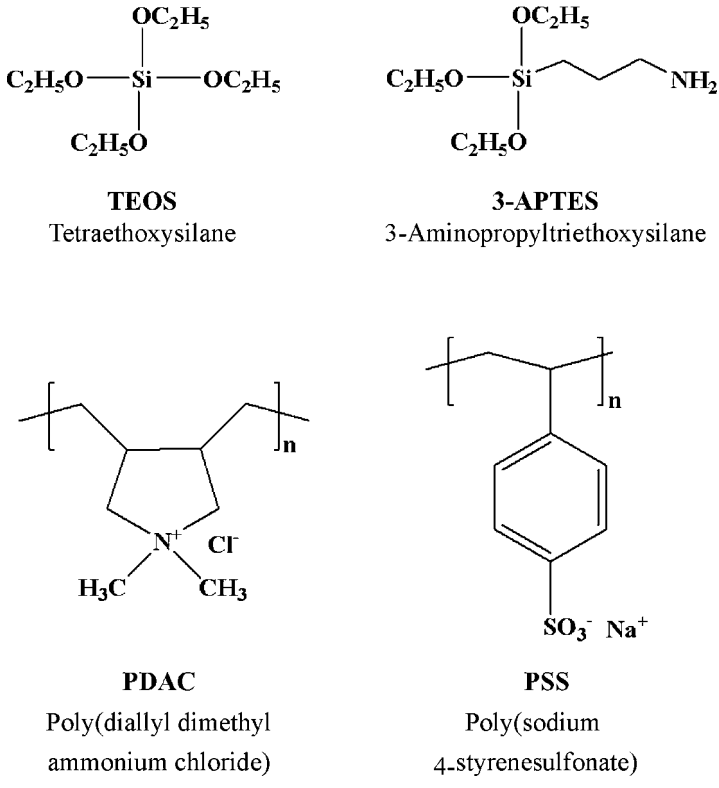

FIGURE 1 Chemical structures of (organo)silicates and polyelectrolytes used in this study.

Preparation of Inorganic Precursors

Inorganic low-molecular-weight precursors were synthesized by the well-known sol-gel method [52]. Ten grams of TEOS was vigorously stirred with 3.42 g of H_2O and 0.05 g of HCl. After the formation of transparent TEOS sol (T-Sol), it was diluted with ethanol (weight ratio of TEOS–ethanol (EtOH) = 3:7). To increase the electrostatic interfacial adhesion between the organic and the inorganic layer, 3-APTES was also added during the synthesis of TEOS sol (1.2 g of 3-APTES and 4.5 g of TEOS were injected into 23.7 g of EtOH), and then 1.42 g of H_2O and 0.6 g of HCl were slowly dropped into the mixture. After an overnight reaction, a clear sol of the reaction product (A-Sol) was obtained. All inorganic sols were filtered with 0.2-μm poly(tetrafluoroethylene) membranes before the LbL deposition.

Fabrication of Organic/Inorganic Hybrid Nanolaminates

Silicon wafers were initially cleaned by treatment with Piranha solution ($H_2SO_4/H_2O_2 = 7/3$ v/v%) for 20 min and the surfaces were sequently negatively charged by heating at 60°C for 15 min in a mixture of $H_2O/H_2O_2/NH_3 = 5/1/1$ v/v%, followed by washing in water and drying with a gentle stream of nitrogen gas. For spin SA multilayer films [25,26], a silicon substrate was completely wetted by a positively charged PDAC solution (10 mM with 0.1 M NaCl). After the solution was dispensed, which typically takes 2–3 s, the substrate was immediately rotated with a spinner at a fixed rotating speed (typically 4000 rpm) for a short period (typically about 15 s). After the film was sufficiently spin-dried at the same speed (typically about 15 s), the substrate was thoroughly rinsed twice with excess deionized water at a speed of 4000 rpm. A negatively charged PSS layer was then deposited onto the substrate containing the positively charged PDAC layer on top using the same procedure. Inorganic layers were deposited onto the spin SA $(PDAC/PSS)_n$ multilayer film by dip coating for 5 min in inorganic precursor sol (T-Sol or A-Sol). Preannealing of [$(PDAC/PSS)_n$/T-Sol or A-Sol] film, enabling the condensation and cross-linking between Si-OH and Si-OC_2H_5 groups, was carried out at 150°C for 30 min [52]. This deposition procedure was repeated for the preparation of [$(PDAC/PSS)_n$/T-Sol or A-Sol]$_4$ film (denoted as T_n or A_n), and the organic/inorganic hybrid film was finally cured at 230°C for 1 h. In the case of A-Sols, the anionic sulfonate group of the PSS layer was electrostatically attached to the amine moieties of the inorganic A-Sol layer. For control experiments, inorganic films not containing any of PE multilayers were also prepared for comparison with the hybrid multilayer films, and these are denoted as $T_{ref(n=0)}$ and $A_{ref(n=0)}$, respectively. A schematic illustration for the preparation of such organic/inorganic hybrid multilayer films is given in Figure 2.

Film Thickness

Ellipsometric thickness measurements were performed using a L2W15S830 ellipsometer (Gaertner Scientific Corp., Skokie, IL, USA) with a 632.8-nm He-Ne laser light source. The thickness difference between the center and the edge is within the experimental error range of ± 1 nm. In addition, the film thickness was measured after cutting off the edge of a silicon wafer covered with mutilayered films. The film thicknesses of individual inorganic layer is fixed at around 110 nm, whereas the thickness of the individual organic PE multilayer [*i.e.*, $(PDAC/PSS)_n$] was varied by changing the number of deposited

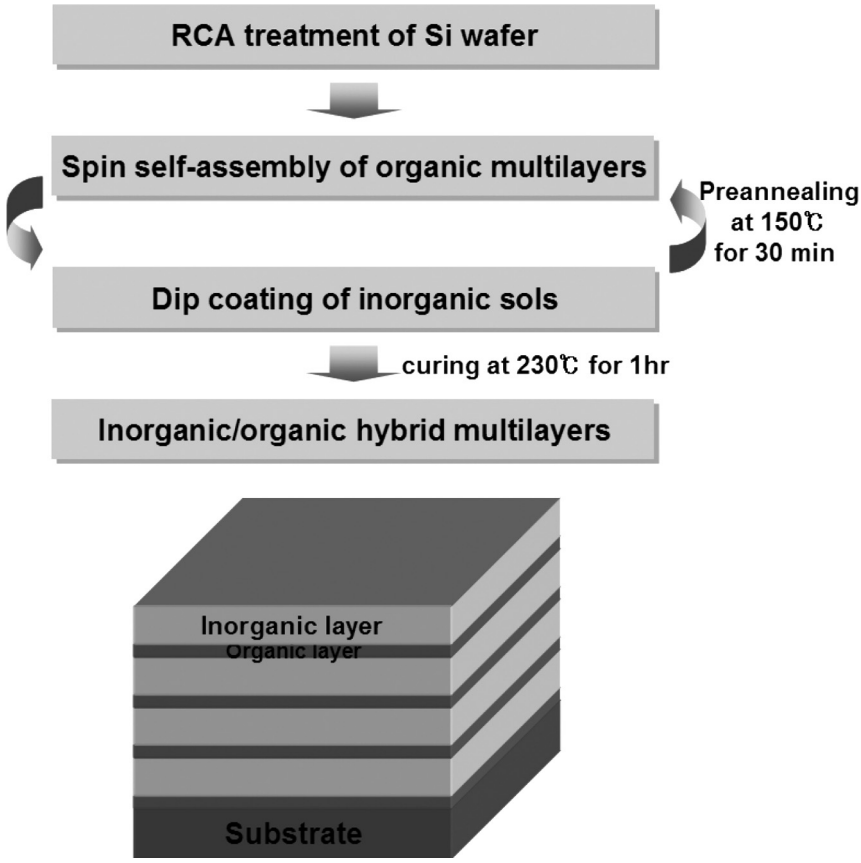

FIGURE 2 Schematic depicting the buildup of organic/inorganic hybrid nanolaminates.

layers (n), indicating the linear relationship between the film thickness and the deposition number. The PE bilayer thickness in both T and A series was measured to be about 4.5 nm. Table 1 summarizes the thicknesses of individual inorganic layers, individual organic multilayers, and organic/inorganic hybrid multilayers measured by ellipsometry.

X-ray Reflectivity

The internal structure of the organic/inorganic hybrid nanolaminates was determined by X-ray reflectivity (XRR) using a Cu Kα ($\lambda = 1.54$ Å) beam at the 3C2 XRD beam line at the Pohang Light Source (PLS),

TABLE 1 Thicknesses of Organic/Inorganic Hybrid Multilayers Measured from Ellipsometry

Film series	Composition of multilayers	Total thickness (nm)	Total thickness of inserted PE organic layers (nm)	Thickness of inorganic layer (nm)
		T-sol series		
T_{ref}	T-sol	485.7	—	—
T_3	$[(PDAC/PSS)_3/T\text{-}sol]_4$	502.1	12.5	113.0
T_4	$[(PDAC/PSS)_4/T\text{-}sol]_4$	526.7	18.7	113.0
T_5	$[(PDAC/PSS)_5/T\text{-}sol]_4$	543.6	22.9	113.0
		A-sol series		
A_{ref}	A-sol	427.4	—	—
A_3	$[(PSS/PDAC)_{2.5}/A\text{-}sol]_4$	485.5	11.3	110.0
A_4	$[(PSS/PDAC)_{3.5}/A\text{-}sol]_4$	498.6	14.7	110.0
A_5	$[(PSS/PDAC)_{4.5}/A\text{-}sol]_4$	546.7	26.7	110.0

Pohang City, Korea, with high-resolution adjustment. The reflectivity tool was employed for fitting the experimental data and extracting parameters such as scattering length density, thickness, and roughness for each layer. Total thickness of the hybrid films is estimated from the small oscillation of Kiessig fringes, and the d-spacing for each organic/inorganic pair is calculated from the Bragg peaks [53].

Mechanical Property

Depth-sensing indentation experiments were performed to determine the apparent modulus, E', and hardness, H, as functions of indentation tip displacement, h, using the continuous stiffness measurement (CSM) technique (Nanoindenter XP II, MTS Corporation, Oak Ridge, TN, USA) with a Berkovich (three-sided pyramid) diamond tip [46]. After E' and H are plotted against the relative displacement (*i.e.*, displacement into the surface with respect to the total film thickness), E' and H values of the films are determined in the plateau region around 0.08–0.1 of the relative displacement to avoid any substrate effect [46]. MicroVickers indentation was also carried out using a HM-124 AKASHI microhardness tester (Akashi, Tokyo, Japan).

Surface Morphology

Optical microscope measurements were carried out using a Nikon OPTIPHOT2-POL in reflection mode. Atomic force microscopic (AFM) measurements were performed by using a Nanoscope IIIa system (Digital Instruments Inc., Buffalo, NY, USA) operating in the tapping mode.

RESULTS AND DISCUSSION

X-ray reflectivity measurement was first conducted based on the significant electron-density difference between organic PE and inorganic layers to characterize the alternating internal structure of the hybrid multilayer films. As shown in Figure 3, X-ray reflectivity spectra of both T_4 and A_4 exhibit evident Bragg peaks, implying the well-ordered organic/inorganic layered structure throughout the film thickness as well as the small oscillation peaks (*i.e.*, Kiessig fringes) originating from the total film thickness [53]. Based on these experimental data, the scattering length density (SLD) profiles can be obtained as shown in the insets of Figure 3, indicating that thick inorganic layers of high SLD are alternatively assembled with thin organic multilayers of relatively low SLD, forming sharp interfaces between the PE and the inorganic layers. The thicknesses of inorganic T-sol and A-sol layers are also calculated to be 112.7 nm and 111.0 nm, respectively, which are in good agreement with the values obtained from ellipsometry. On the other hand, the thicknesses of PE multilayers determined from the reflectivity measurements (*i.e.*, 14.0 nm for T_4 and 12.4 nm for A_4) are somewhat smaller than the values obtained from the ellipsometric measurements (18.7 nm for T_4 and 14.7 nm for A_4), presumably due to the slight deviation of experimental data from the curve fitting in X-ray reflectivity.

To investigate the fundamental mechanical behavior of organic/inorganic hybrid nanolaminates, depth-sensing indentation experiments were performed in CSM mode [46]. Figure 4 shows the load (P)–displacement (h) curves of T- and A-series samples during loading and unloading cycles of the tip. After unloading, the displacement of the tip was set to be around 400 nm of depth in all cases. All the load curves evidently indicate that all the films show elastic–plastic deformation [46,54]. Furthermore, more displacement of the tip occurs for the same load at the initial stage of loading (about 10% depth of the total film thickness) when the thickness of inserted organic multilayer is increased, as evidenced in the insets of Figure 4. This deformation behavior indicates that the plastic mechanical behavior of the hybrid multilayer films is amplified as the inserted amount of the organic PE multilayers is gradually increased [46]. At the middle stage of the loading curve, the small deviations or stretches in the load curves, typically known to originate from plastic deformations [55–59], such as crack initiation, fracture propagation, pile-up, or yielding, start to show up in all the samples except for $T_{ref(n=0)}$ and $A_{ref(n=0)}$ reference samples.

For better understanding of these deviations or stretches in the load curves, expanded and shifted load curves highlighting the initial and

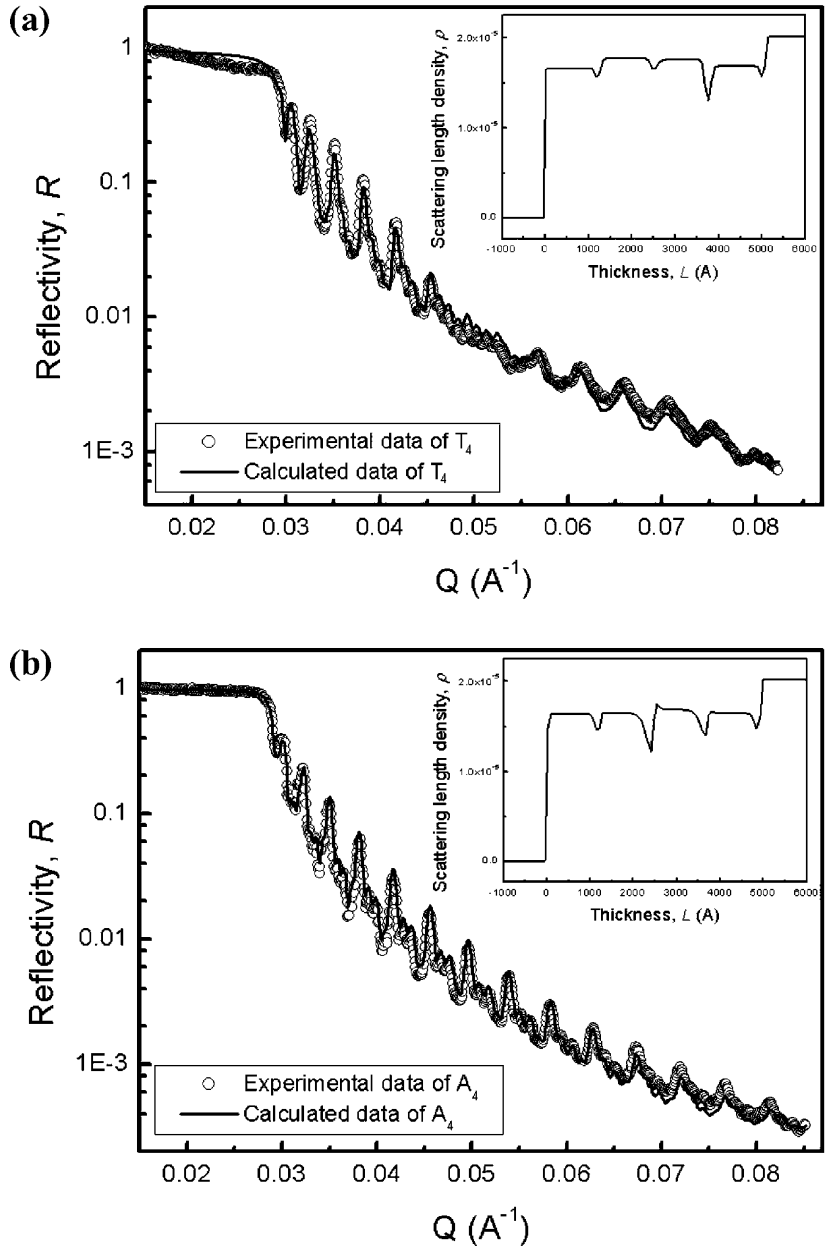

FIGURE 3 X-ray reflectivity spectra of (a) T_4 and (b) A_4. The insets show the scattering length density profiles of (a) T_4 and (b) A_4.

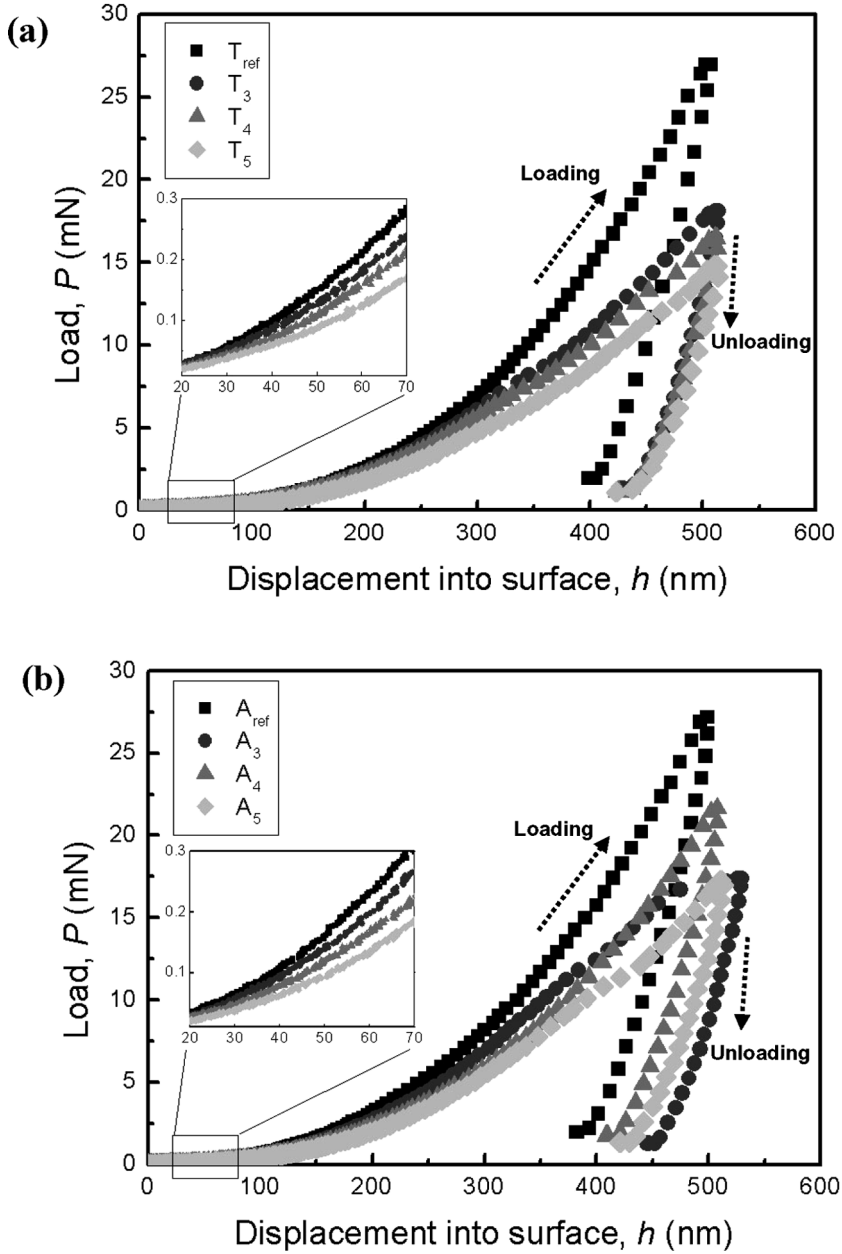

FIGURE 4 Load-displacement curves of (a) T_n series and (b) A_n series with $n = 0$, 3, 4, and 5.

middle stages of the loading are shown in Figure 5 (for the guidance of the eye, the curves of $n = 3$ (T_3 and A_3), $n = 4$ (T_4 and A_4), and $n = 5$ (T_5 and A_5) are shifted to 100, 200, and 300 nm to the right-hand side, respectively). It should be noted here that each curve fitting using the power law equation [46] is in agreement with the measured loading curve up to a certain point (indicated by an arrow), above which the fitting slightly deviates from the measured loading curve [59]. Thus, the load at this point is defined as the *critical load* that is believed to cause the initiation of plastic deformations as mentioned previously [55–59]. Based on this definition, the critical loads are found to be 8.3 mN for T_3, 7.1 mN for T_4, and 5.2 mN for T_5 for the T-series samples and 11.2 mN for A_3, 10.9 mN for A_4, and 10.4 mN for A_5 for the A-series samples. It is observed that the critical load decreases with increasing organic layer thickness because of the plastic characteristics of the inserted organic layers in both T series and A series. Additionally, the decrease in critical loads of the T_n series (*i.e.*, 37.3% decrease from T_3 to T_5) is relatively higher than the decrease in the A_n series (*i.e.*, 7.1% decrease from A_3 to A_5). Taking into account the fact that the thicknesses of PE layers in the T_n sample series are similar to those in the corresponding A_n series, it is believed that the relatively small decrease in the critical loads shown in the A_n series originates from the strong intermolecular interaction at the interface between organic and inorganic layers. This assumption is supported by the fact that the A_n samples have relatively strong electrostatic interaction between the inorganic layer consisting of TEOS/3-APTES carrying cationic amine groups and the anionic PSS organic layer, in comparison with the T_n series samples containing pure TEOS and PE multilayers, although the charge density of the mixed inorganic layer (TEOS and 3-APTES) is not quantitatively determined in this study.

The apparent modulus and hardness of (a) T series and (b) A series are plotted against the relative displacement (h/t_f), defined as the tip displacement toward the substrate relative to total film thickness, as shown in Figure 6. Small perturbations originating from the initial contact of a indenter tip with the surface of multilayers typically appear at the early stage of a relatively shallow depth (more specifically, 0–0.05 or 0.07) of relative displacement. However, as the relative displacement is increased, plateau regions are reached with minimal fluctuation in measured mechanical values, reflecting intrinsic properties of the film. Further increase in the relative displacement significantly increases both E' and H because of the substrate effect. The apparent modulus and hardness values reported in this study are averaged within 8–10% depth of the total film thickness, which is not affected by the substrate [46,55,56].

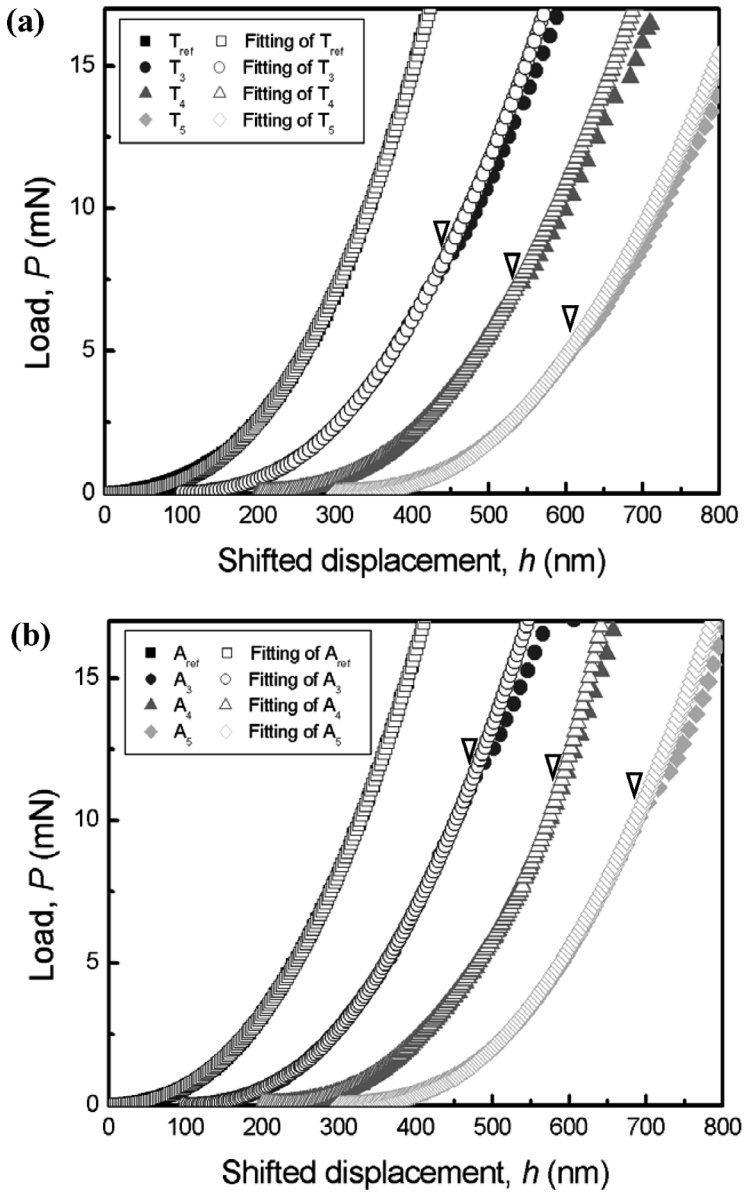

FIGURE 5 Expanded and shifted load-displacement curves of (a) T_n series and (b) A_n series with $n = 0$, 3, 4, and 5. Respective curves are shifted for eye guidance to the x-axis; 100 nm for T_3 and A_3; 200 nm for T_4 and A_4; 300 nm for T_5 and A_5.

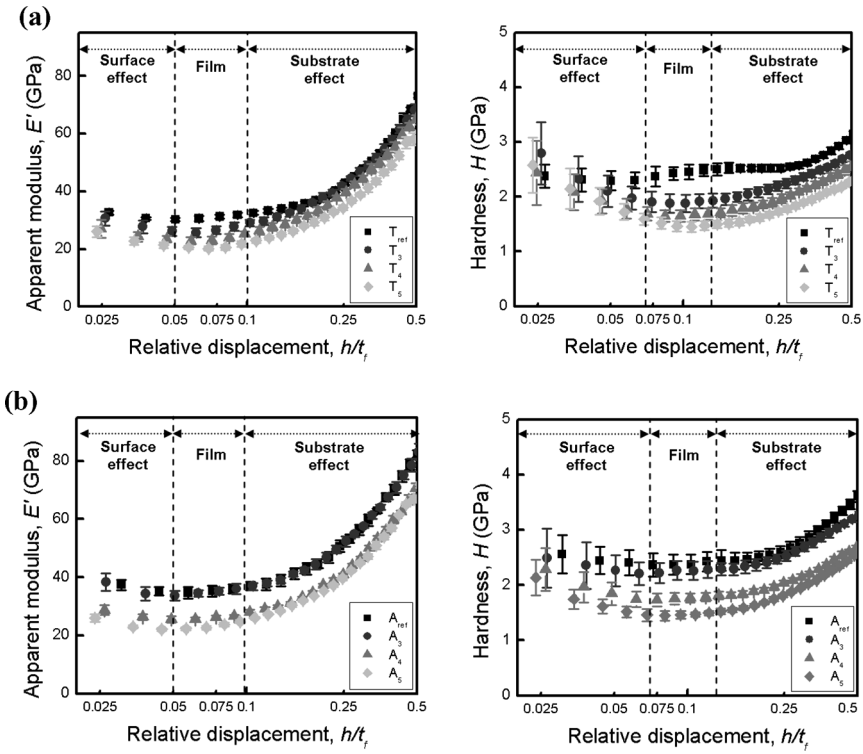

FIGURE 6 Apparent modulus and hardness curves of (a) T series and (b) A series as a function of relative displacement.

Figure 7 shows the relationship between mechanical properties of organic/inorganic hybrid thin films and the thickness of inserted PE layers. As the PE bilayer number is increased from zero to five bilayers, the apparent modulus (E') and hardness (H) almost linearly decrease in both T_n and A_n samples. This trend shown in E' and H indicates that the final mechanical properties of organic/inorganic hybrid nanolaminates decrease in proportion to the amount of inserted PE multilayers, presumably because of the dominance of organic layers with relatively low E' and H values compared with those of inorganic silicate layers [1,2]. More specifically, the decrease in E' per organic layer thickness (nm) in each organic multilayer is 0.39 GPa and 0.48 GPa for the T_n and A_n series, respectively. Also, the decrease in hardness, H, per organic layer thickness (nm) in each organic multilayer is estimated to be 0.043 GPa and 0.034 GPa for the T_n and A_n series, respectively. The ratios of decreased E' to decreased H (E'/H)

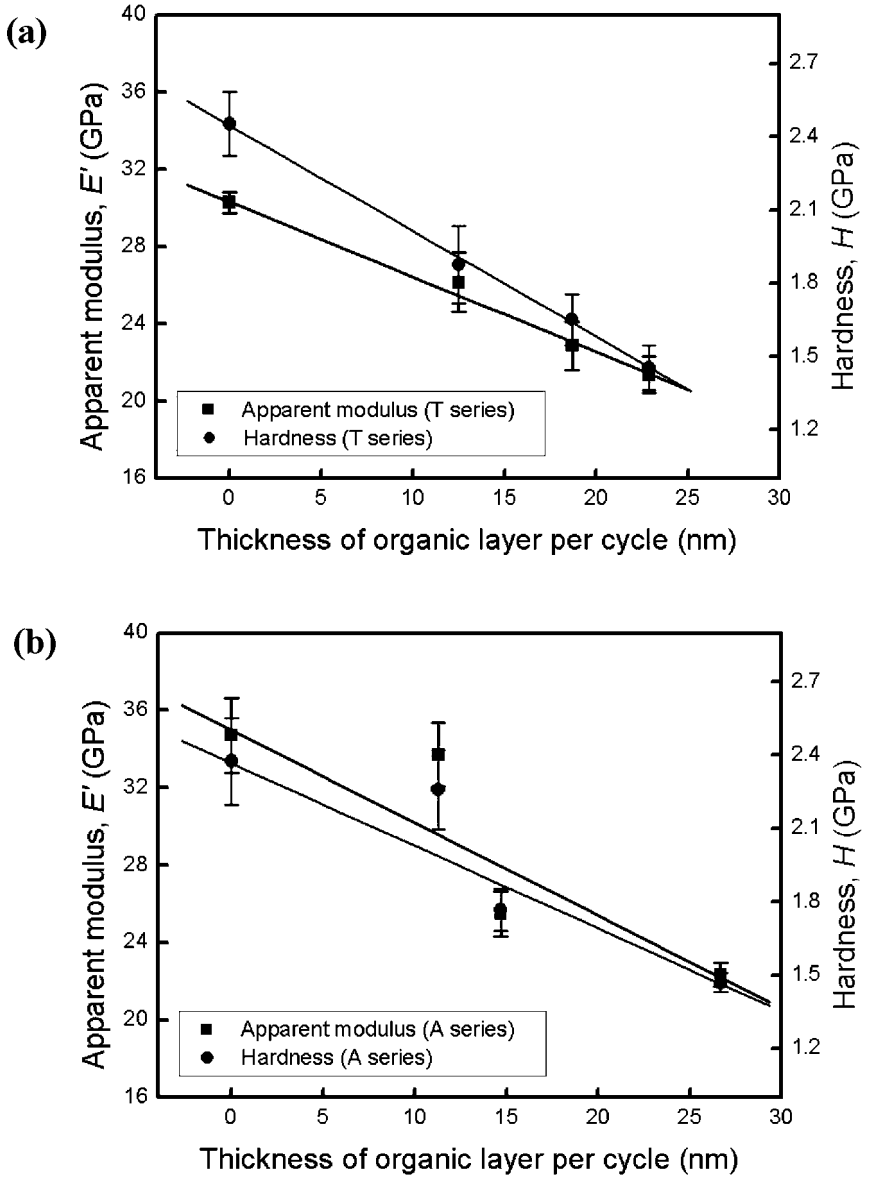

FIGURE 7 Apparent modulus and hardness curves of (a) T_n series and (b) A_n series with different thickness of inserted PE layers.

per organic layer thickness are 9.1 for the T_n series samples and 14.1 for the A_n series samples. The relatively high value of the decreased E'/H ratio shown in the A_n series implies that the A_n series samples lose more elastic energy to recover from a given displacement or, in other words, absorb more deformation energy in comparison with the T series samples [60,61]. This result reflects that the energy dissipation by the insertion of organic layers is more effective in the A_n than in the T_n series samples.

To quantitatively estimate the fracture toughness of the hybrid multilayer films, crack lengths of at least 10 points were measured using optical microscopy (OM) with image analysis program after indentation with a microVickers [47–49]. In this case, each crack length was obtained from the distance from the center of an indentation mark to the end of the crack. As shown in Figure 8, the cracks propagate from the corners of indentation marks after a loading of 980 mN. The area near the indentation mark in T_{ref} is fully delaminated, but the stress-loaded areas of the $T_{n=3\sim5}$ samples are ruptured by the indentation (Figure 8a). In terms of the crack length formed upon indentation, $T_{ref(n=0)}$ has the longest crack length of $16.4 \pm 1.5\,\mu m$ among the T_n series tested, and the other T_n series samples with $n = 3$, 4, and 5 have a similar crack length of about $14 \pm 1.0\,\mu m$ within the experimental error, as shown in Figure 8a. On the other hand, crack length decreases from $16.3 \pm 0.5\,\mu m$ for the A_{ref} to $12.2 \pm 1.6\,\mu m$ with increasing the number of inserted PE layers in each organic layer. As a result, the T_n series samples show the fracture and delamination behavior rather than releasing fracture energy, and the inserted PE layers in the A_n series serve as resistance layers against the crack propagation and the rupture of the films.

Based on E', H, and the crack length obtained from the T_n and A_n series, the fracture toughness (K_{IC}) is calculated using the following equation [47–51,62]. Even though various types of mechanical testing methods to evaluate the fracture toughness, such as bending, buckling, scratching, and tensile testing, have been used, the method adopted in the present study is selected to take full advantage of its simple and straightforward approach [63].

$$K_{IC} = \alpha \left(\frac{E}{H}\right)^{1/2} \left(\frac{P}{l_{crack}^{3/2}}\right)$$

where α is the empirical constant dependent on the tip geometry (typically, 0.016 in our case), E ($\approx E'$) is the elastic modulus [46], H is the hardness, P is the applied load, and l_{crack} is the crack length propagating from the center of an indentation impression. Although this

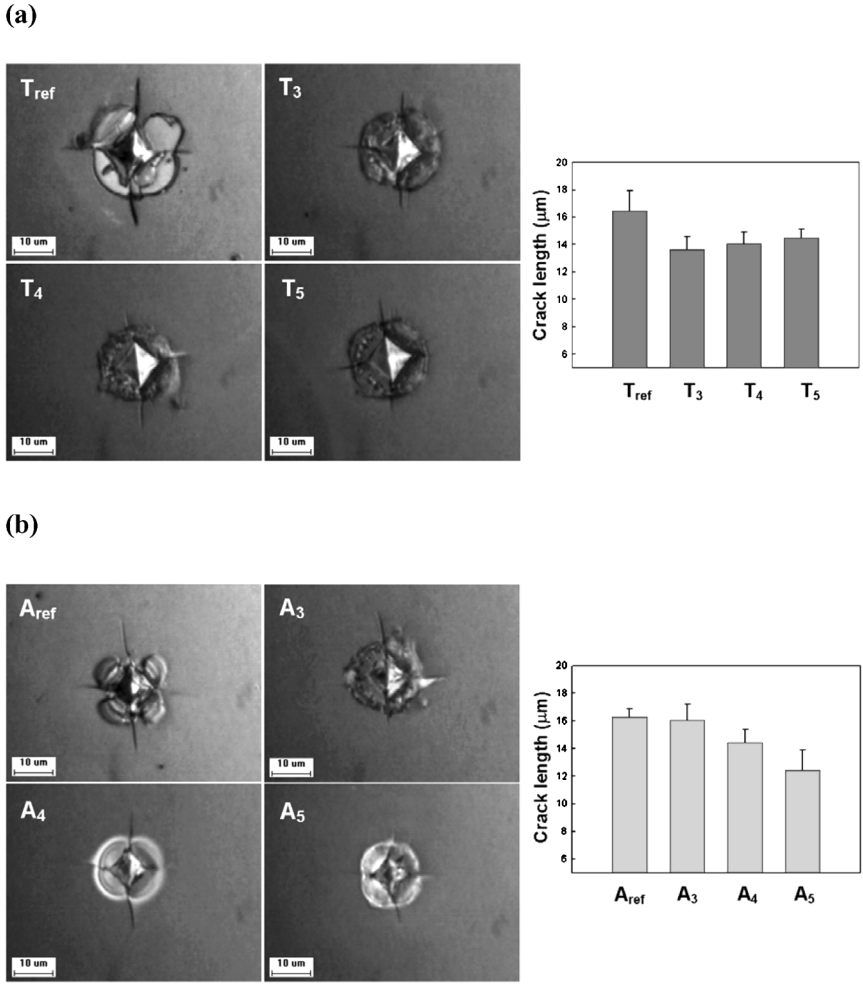

FIGURE 8 Optical microscope images of crack-formation and crack-length measurements after loading 980 mN of microVickes indentations for (a) T_n series and (b) A_n series with $n = 0$, 3, 4, and 5.

equation has been widely used for various kinds of single- or multilayer films ranging from nano (or micro) to bulk scale, the accuracy or validity of the equation is not fully proven [64]. However, we could qualitatively estimate the fracture toughness of multilayer thin films by fixing other variables such as total film thickness, the kind of substrate, and applied load.

Figure 9 indicates that the fracture toughness for both T_n and A_n series thin films increases when PE organic layers are inserted in between the inorganic films. However, it is noted that although all the fracture toughness values estimated for the $T_{n=3\sim5}$ series samples have similar values around 1.1 MPa·$m^{0.5}$ as shown in Figure 9a, the fracture toughness of the A_n series significantly increases with the increase in the thickness of inserted PE layers in each organic layer, as evidenced in Figure 9b. Based on these results obtained from both T_n and A_n series samples, the T_n series samples show the fracture and delamination behavior with low fracture toughness (about 1.1 MPa·$m^{0.5}$) due to the weak electrostatic interaction between the PE and the inorganic layers. Although the electrostatic interaction between silanol groups (Si-OH) of the T-Sol and quaternary amine groups of PDAC initially drives the buildup of the PE multilayers onto the T-Sol layer, the heat treatment of the hybrid films at 230°C for 1 h could possibly eliminate many electrostatic bonding sites due to the condensation and cross-linking of the silanol groups and, eventually, yield partial electrostatic interaction at the interface [52]. However, the inserted PE layers in the A_n series samples are electrostatically associated with the inorganic layers carrying amine moieties as well as silanol groups, and these organic layers can serve as resistance layers, even after heat treatment, against crack propagation and deformation, yielding the relatively high fracture toughness of 1.52 MPa·$m^{0.5}$.

Further evidence on the effect of interfacial adhesion can be provided by the morphology of indentation impressions after the indentation at a 500-nm depth measured with atomic force microscopy (AFM), as represented in Figure 10. First, both reference $T_{ref(n=0)}$ and $A_{ref(n=0)}$ samples show little or no pile-ups around the indentation marks, which are believed to be due to the elastic deformation of the samples without inserted organic multilayers [62–64]. In the case of T_5, however, visible long cracks and a pile-up of the film material around the indentation mark are formed, implying that the low interfacial adhesion has difficulty in dissipating mechanical stress and fracture energy into the PE as well as the inorganic layers. On the other hand, for the A_5 sample, an evident pile-up near the indentation mark is observed, indicating that the inserted PE layers are strongly associated with the inorganic layers acting as plasticizers (or stress releasers) without any cracks being developed around the indentation [5,6]. In addition, the height profiles shown in Figure 10e evidently support these observations. The arrows indicate the locations of a pile-up for each sample. The lateral displacement of the pile-up (*i.e.*, the distance from the center of the indentation mark to the end of a pile-up) is

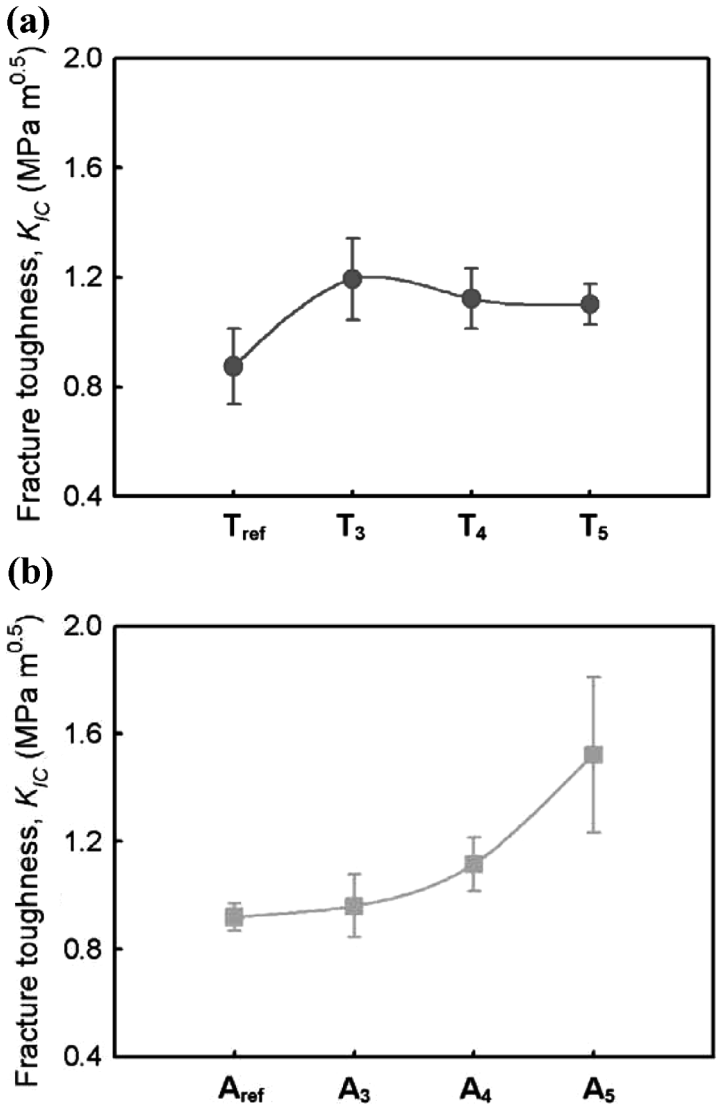

FIGURE 9 Change in fracture toughness with the increase in PE thickness in each organic layer for (a) T_n series and (b) A_n series with $n = 0$, 3, 4, and 5.

measured to be 2.7 μm for T_5 and 2.1 μm for A_5. This AFM observation implies that the larger lateral displacement of such a pile-up in T_5 compared with the corresponding value in A_5 is caused by the weak interfacial adhesion between the PE organic and the inorganic layers.

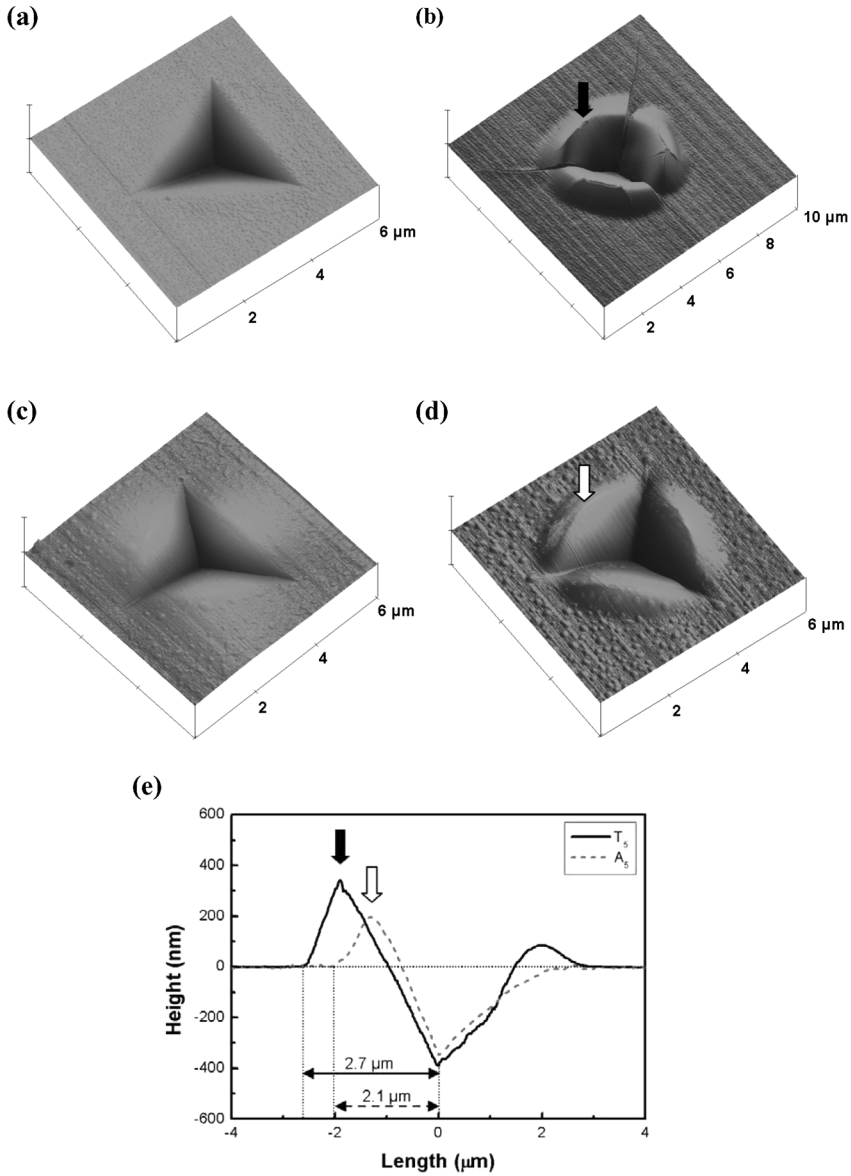

FIGURE 10 AFM images of indentation impressions of (a) $T_{ref(n=0)}$, (b) T_5, (c) $A_{ref(n=0)}$, and (d) A_5 after 500-nm depth indentations along with the height profile of T_5 and A_5 (e). All the height scales from (a) to (d) are 500 nm/division.

CONCLUSIONS

We prepared PE/silicate hybrid nanolaminates using the LbL method based on the electrostatic intermolecular interaction. We further demonstrated with two different types of nanolaminates with varying degrees of electrostatic interaction that the interfacial adhesion in nanolevel thickness could significantly improve the fracture toughness of hybrid multilayer films. The strong interfacial interaction between PE and silicate causes a significant increase in the fracture toughness of the hybrid multilayers with an increase in the thickness of inserted organic layers because the plastic property of the PE organic layers redistributes the stress concentration and dissipates the fracture energy, resulting in short crack length and high fracture toughness. However, relatively low interfacial interaction between the PE and the inorganic layers, as shown in the T-series samples, has no appreciable influence on the improvement in mechanical properties such as fracture toughness and crack length. We believe that this notion of the importance of interfacial adhesion in organic/inorganic multilayered nanolaminates can be widely applied to many reinforcing agents, adhesives or building materials requiring high mechanical strength and crack resistance.

ACKNOWLEDGMENT

This work was financially supported by the National Research Laboratory Program (Grant M1-0104-00-0191) and funded in part by the Ministry of Education through the Brain Korea 21 Programs at Seoul National University. Additionaly, this work was supported by the SRC/ERC program of MOST/KOSEF (R11-2005-048-00000-0). B. Y. also acknowledges the financial support through the Seoul Science Fellowship. The X-ray experiments performed at Pohang Light Source were supported by the Ministry of Science and Technology of Korea (MOST).

REFERENCES

[1] Currey, J. D., *Proc. R. Soc. Lond. B* **196**, 443–463 (1977).
[2] Jackson, A. P., Vincent, J. F., and Turner, R. M., *Proc. R. Soc. Lond. B* **234**, 415–440 (1988).
[3] Sarikaya, M. and Aksay, I. A., *Design and Processing of Materials by Biomimetics* (Americal Institute of Physics, New York, 1995).
[4] Shaffer, T. E., Ionescu-Zanetti, C., Proksch, R., Fritz, M., Walters, D. A., Almqvist, N., Zaremba, C. M., Belcher, A. M., Smith, B. L., Stucky, G. D., Morse, D. E., and Hansma, P. K., *Chem. Mater.* **9**, 1731–1740 (1997).

[5] Evans, A. G., Suo, Z., Wang, R. Z., Aksay, I. A., He, M. Y., and Hutchinson, J. W., *J. Mater. Res*. **16**(9), 2475–2484 (2001).
[6] Wang, R. Z., Suo, Z., Evans, A. G., Yao, N., and Aksay, I. A., *J. Mater. Res*. **16**(9), 2485–2493 (2001).
[7] Li, X., Chang, W.-C., Chao, Y. J., Wang, R., and Chang, M., *Nano Letters* **4**(4), 613–617 (2004).
[8] Smith, B. L., Schaffer, T. E., Viani, M., Thompson, J. B., Frederick, N. A., Kindt, J., Belcher, A., Stucky, G. D., Morse, D. E., and Hansma, P. K., *Nature* **399**(24), 761–763 (1999).
[9] Weiss, I. M., Renner, C., Strigl, M. G., and Fritz, M., *Chem. Mater*. **14**, 3252–3259 (2002).
[10] Wustman, B. A., Morse, D. E., and Evans, J. S., *Langmuir* **18**, 9901–9906 (2002).
[11] Sudo, S., Fujikawa, T., Nagakura, T., Ohkubo, T., Sakaguchi, K., Tanaka, M., Nakashima, K., and Takahashi, T., *Nature* **387**, 563–564 (1997).
[12] Zaremba, C. M., Belcher, A. M., Fritz, M., Li, Y., Mann, S., Hansma, P. K., Morse, D. E., Speck, J. S., and Stucky, G. D., *Chem. Mater*. **8**, 679–690 (1996).
[13] Xu, G., Yao, N., Aksay, I. A., and Groves, J. T., *J. Am. Chem. Soc*. **120**, 11977–11985 (1998).
[14] Aizenberg, J., Black, A. J., and Whitesides, G. M., *J. Am. Chem. Soc*. **121**, 4500–4509 (1999).
[15] Kato, T., Sugawara, A., and Hosoda, N., *Adv. Mater*. **14**(12), 869–877 (2002).
[16] Hosoda, N., Sugawara, A., and Kato, T., *Macromolecules* **36**, 6449–6452 (2003).
[17] Naka, K. and Chujo, Y., *Chem. Mater*. **13**, 3245–3259 (2001).
[18] Falini, G., Albeck, S., Weiner, S., and Addadi, L., *Science* **271**, 67–69 (1996).
[19] Aizenberg, J., Muller, D. A., Grazul, J. L., and Hamann, D. R., *Science* **299**, 1205–1208 (2003).
[20] Loste, E., Park, R. J., Warren, J., and Meldrum, F. C., *Adv. Func. Mater*. **14**(12), 1211–1220 (2004).
[21] Hirai, T., Hariguchi, S., and Komasawa, I., *Langmuir* **13**, 6650–6653 (1997).
[22] Decher, G., Hong, J. D., and Schmitt, J., *Thin Solid Films* **210**, 831–835 (1992).
[23] Decher, G., *Science* **277**(29), 1232–1237 (1997).
[24] G. Decher and J. B. Schlenoff (Eds.), *Multilayer Thin Films* (Wiley-VCH, Weinheim, 2003).
[25] Cho, J., Char, K., Hong, J., and Lee, K., *Adv. Mater*. **13**(14), 1076–1078 (2001).
[26] Cho, J. and Char, K., *Langmuir* **20**, 4011–4016 (2004).
[27] Cho, J. and Char, K., *Korean J. Chem. Eng*. **20**(1), 174–179 (2003).
[28] Jang, H., Kim, S., and Char, K., *Langmuir* **19**, 3094–3097 (2003).
[29] Cho, J., Lee, S-H., Kang, H., Char, K., Koo, J., Seung, B. H., and Lee, K.-B., *Polymer* **44**, 5455–5459 (2003).
[30] Cho, J., Char, K., and Kim, D. Y., *Thin Solid Films* **415**, 303–307 (2002).
[31] Lee, I., Ahn, J. S., Hendricks, T. R., Rubner, M. F., and Hammond, P. T., *Langmuir* **20**, 2478–2483 (2004).
[32] Maehara, Y., Takenaka, S., Shimizu, K., Yoshikawa, M., and Shiratori, S., *Thin Solid Films* **438–439**, 65–69 (2003).
[33] Ding, H., Ram, M. K., and Nicolini, C., *J. Mater. Chem*. **12**, 3585–3590 (2002).
[34] Khomutov, G. B., Beresneva, I. V., Bykov, I. V., Gainutdinov, R. V., Koksharov, Y. A., Mantsyzov, B. I., Masselin, P., Ozheredov, I. A., Radchenkko, I. L., Shkurinov, A. P., and Tolstikhina, A. L., *Colloids and Surfaces A—Physicochemical and Engineering Aspects* **198–200**, 491–499 (2002).
[35] Hammond, P. T., *Adv. Mater*. **16**, 1271–1293 (2004).
[36] Yang, S. Y. and Rubner, M. F., *J. Am. Chem. Soc*. **124**, 2100–2101 (2002).

[37] Ho, P. K. H., Kim, J.-S., Burroughs, J. H., Becker, H., Li, S. F. Y., Brown, T. M., Cacialli, F., and Friend, R. H., *Nature* **404**, 481–484 (2000).
[38] Ho, P. K. H., Granstrom, M., Friend, R. H., and Greenham, N. C., *Adv. Mater*. **10**, 769–774 (1998).
[39] Rmaile, H. H. and Schlenoff, J. B., *J. Am. Chem. Soc*. **125**, 6602–6603 (2003).
[40] Hiller, J., Mendelsohn, J. D., and Rubner, M., *Nature Materials* **1**, 59–63 (2002).
[41] Wang, T. C., Cohen, R. E., and Rubner, M. F., *Adv. Mater*. **14**, 1534–1537 (2002).
[42] Caruso, F., Caruso, R. A., and Möhwald, H., *Science* **282**, 1111–1114 (1998).
[43] Fan, X., Park, M.-K., Xia, C., and Advincula, R., *J. Mater. Res*. **17**(7), 1622–1633 (2002).
[44] Tang, Z., Kotov, N. A., Magonov, S., and Ozturk, B., *Nature Materials* **2**, 413–418 (2003).
[45] He, J. L., Li, W. Z., Li, H. D., Wang, J., and Wang, L. D., *Surface and Coatings Technology* **103–104**, 109–112 (1998).
[46] Oliver, W. C. and Pharr, G. M., *J. Mater. Res*. **7**(6), 1564–1583 (1992).
[47] Lawn, B. R., Evans, A. G., and Marshall, D. B., *J. Am. Ceram. Soc*. **63**(9–10), 574–581 (1980).
[48] Pharr, G. M., Harding, D. S., and Oliver, W. C., *Mechanical Properties and Deformation Behavior of Materials Having Ultra-fine Microstructures* (Kluwer, Dordrecht, Netherlands, 1993), pp. 449–461.
[49] Anstis, G. R., Chantikol, P., Lawn, B. R., and Marshall, D. B., *J. Am. Ceram. Soc*. **64**(9), 533–538 (1981).
[50] Harding, D. S., Oliver, W. C., and Pharr, G. M., *MRS Symposium Proceedings* **356**, 663–668 (1995).
[51] Gerberich, W. W., Jungk, J. M., Li, M., Volinsky, A. A., Hoehn, J. W., and Yoder, K., *International Journal of Fracture* **119–120**, 387–405 (2003).
[52] Brinker, C. J. and Sherer, G. W., *Sol-Gel Science* (Academic Press, New York, 1990).
[53] Russell, T. P., *Materials Science Reports* **5**, 171–271 (1990).
[54] Street, S. C., Rar, A., Zhou, J. N., Liu, W. J., and Barnard, J. A., *Chem. Mater*. **13**, 3669–3677 (2001).
[55] Kim, S., Toivola, Y., Cook, R. F., Char, K., Chu, S-H., Lee, J.-K., Yoon, D. Y., Rhee, H.-W., *J. Electochem. Soc*. **151**(3), F37–F44 (2004).
[56] Toivola, Y., Kim, S., Cook, R. F., Char, K., Lee, J.-K., Yoon, D. Y., Rhee, H.-W., Kim, S. Y., and Jin, M. Y., *J. Electochem. Soc*. **151**(3), F45–F53 (2004).
[57] Toivola, Y., Thurn, J., and Cook, R. F., *J. Electochem. Soc*. **149**(3), F9–F17 (2002).
[58] Gerberich, W. W., Jungk, J. M., Li, M., Volinsky, A. A., Hoehn, J. W., and Yoder, K., *International Journal of Fracture* **119–120**, 387–405 (2003).
[59] Schuh, C. A., Mason, J. K, and Lund, A. C., *Nature Materials* **4**, 617–621 (2005).
[60] Alcala, J., Barone, A. C., and Anglada, M., *Acta Mater*. **48**, 3451–3464 (2000).
[61] Marx, V. and Balke, H., *Acta Mater*. **45**, 3791–3800 (1997).
[62] Karimi, A., Wang, Y., Cselle, T., and Morstein, M., *Thin Solid Films* **420–421**, 275–280 (2002).
[63] Zhang, S., Sun, D., Fu, Y., and Du, H., *Surface and Coatings Technology* **198**, 74–84 (2005).
[64] Vella, J. B., Adhihetty, I. S., Junker, K., and Volinsky, A. A., *International Journal of Fracture* **119–120**, 487–499 (2003).
[65] Street, S. C., Rar, A., Zhou, J. N., Liu, W. J., and Barnard, J. A., *Chem. Mater*. **13**, 3669–3677 (2001).
[66] Pavoor, P. V., Bellare, A., Strom, A., Yang, D., and Cohen, R. E., *Macromolecules* **37**, 4865–4871 (2004).
[67] Du, B., Tsui, O. K. C., Zhang, Q., and He, T., *Langmuir* **17**, 3286–3291 (2001).